Neutron scattering study of magnetic excitations in $YBa_2Cu_3O_{6+x}$

J. M. Tranquada and G. Shirane
Physics Department, Brookhaven National Laboratory, Upton, New York 11973

B. Keimer
Center for Materials Science and Engineering, Massachusetts Institute of Technology, Cambridge, Massachusetts 02139

S. Shamoto and M. Sato
Institute for Molecular Science, Okazaki 444, Japan
(Received 17 April 1989)

Inelastic neutron scattering has been used to study magnetic excitations in several single crystals of $YBa_2Cu_3O_{6+x}$. In particular, an extensive study of spin waves in a large crystal with $x=0.3$ has been performed. As in La_2CuO_4, a very large superexchange is found within the CuO_2 layers, with $J_{\parallel}=80^{+60}_{-30}$ meV. The optical-mode spin-wave energies are higher than 30 meV, indicating that $J_{\perp 1}$, the coupling between nearest-neighbor CuO_2 planes, is $\gtrsim 2$ meV. From the dispersion and splitting of the acoustic modes, we obtain values of 0.020 ± 0.005 meV for the effective exchange between next-nearest-neighbor layers, $J_{\perp 2}$, and 0.035 ± 0.005 meV for the anisotropy parameter D. The weak anisotropy gives the planes an XY-like symmetry; no evidence has been found for any in-plane anisotropy. The CuO_2 bilayers remain strongly correlated well above T_N, and dispersion of the acoustic modes appears 30 K above T_N. The decrease of the magnetic order parameter below 30 K in the $x=0.3$ crystal is interpreted as the onset of an incoherent ordering of Cu moments in the oxygen-deficient CuO_x layers. Low-energy inelastic scattering associated with the transition is also observed. Searches for low-energy magnetic fluctuations in several superconducting single crystals have so far been unsuccessful.

I. INTRODUCTION

There is an intimate connection between antiferromagnetism and superconductivity in layered copper oxide compounds. A crossover from an antiferromagnetic insulator phase to the metallic superconducting regime is observed in the systems

$$La_{2-x}(Sr,Ba)_xCuO_4\ ,\quad YBa_2Cu_3O_{6+x}\ ,$$

$$Bi_2Sr_2Ca_xY_{1-x}Cu_2O_8\ ,\ \text{and}\ TlBa_2Ca_xY_{1-x}Cu_2O_7$$

as the doping variable x is increased.[1-6] The transition from magnetic order to superconductivity is relatively sharp, although a spin-glass phase sometimes intervenes.[7] The magnetic ordering occurs due to the large intrasite Coulomb energies on the Cu atoms and the unusually strong superexchange interactions between neighboring Cu atoms via the intervening oxygens in the CuO_2 planes which are a structural element common to all of these materials.

Whether or not magnetism is directly related to the mechanism responsible for superconductivity, it is certainly an important symptom of the strong electronic correlations that exist and that must be taken into account in any successful theory of electron pairing in the cuprates. Thus, the magnetic properties of these materials have received a considerable amount of attention. Of particular interest are the excitation spectra, from which one can determine magnetic interaction strengths and spin-spin correlation lengths.

Most of the inelastic scattering studies performed so far have been on $La_{2-x}Sr_xCuO_4$. The first exciting discovery was the observation[8] that the two-dimensional (2D) magnetic correlations in the CuO_2 planes in La_2CuO_4 survive well above the Néel temperature T_N due to the large in-plane superexchange interaction. Subsequent studies[9] showed that although the long-range order is rapidly eliminated by the introduction of holes via doping with Sr or O, Cu spins within the same plane remain correlated with a fairly short spin-spin correlation length. Muon-spin-rotation studies,[10] together with the neutron scattering work,[9] indicate that the Cu atoms maintain their magnetic moments in the presence of holes.

Unlike La_2CuO_4, the CuO_2 planes in $YBa_2Cu_3O_{6+x}$ are grouped in pairs (bilayers) as shown in Fig. 1(a). Despite this difference we expect the dynamics to be dominantly two dimensional. Figure 1(b) shows the (hhl) scattering plane in which we have performed all of our neutron scattering measurements. If the spin waves in a magnetically ordered sample were completely 2D, then there would be no dispersion along the $(\frac{1}{2},\frac{1}{2},l)$ scattering rod.[11] Holding the neutron energy transfer ΔE fixed, a scan of type A [see Fig. 1(b)] should intersect two steep dispersion surfaces at $+|q_{2D}|$ and $-|q_{2D}|$, where $q_{2D}=\Delta E/c$, and the dispersion slope c is determined by the in-plane superexchange constant $J_{\parallel}$. Although our spectrometer resolution was not sufficient to resolve the two spin-wave branches, our initial measurements[12] (see Fig. 2) on a single crystal with $x\sim0.15$ were consistent with a minimum spin-wave velocity of 0.5 eV Å. This value corresponds to a lower limit for $J_{\parallel}$ of ~ 90 meV, in reasonable agree-

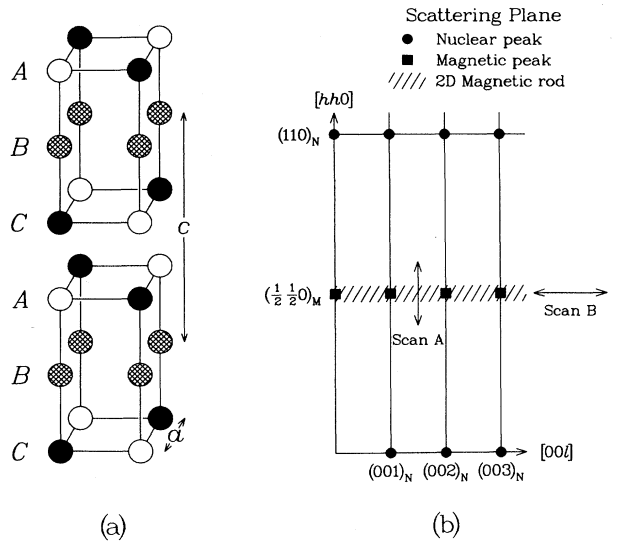

FIG. 1. (a) Magnetic spin arrangement in $YBa_2Cu_3O_{6+x}$ with x near zero. Cross-hatched circles represent nonmagnetic Cu^{1+} ions, while solid and open circles indicate antiparallel spins at Cu^{2+} sites. (b) Reciprocal space (hhl) zone. The hatched line along $(\frac{1}{2},\frac{1}{2},l)$ is the magnetic ridge for two-dimensional scattering, and A and B indicate scans across and along the ridge, respectively.

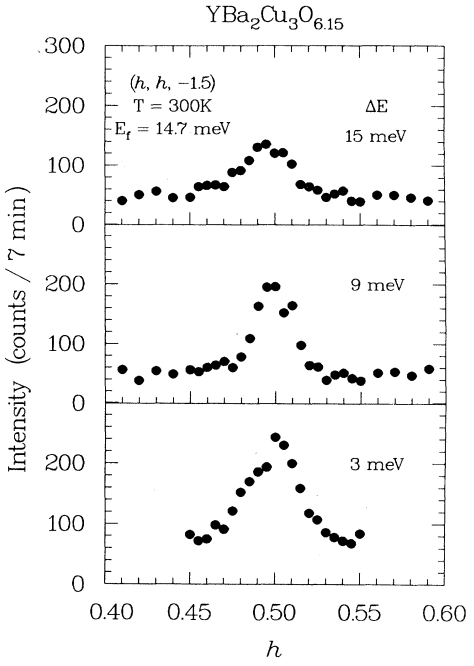

FIG. 2. Several constant ΔE scans across the 2D magnetic ridge in $YBa_2Cu_3O_{6.15}$ (crystal 1) as indicated by scan A in Fig. 1(b). The zone center for 2D spin waves is along $(\frac{1}{2},\frac{1}{2},l)$. The intensities have been adjusted slightly to correct for the presence of $\lambda/2$ contamination seen by the incident-beam monitor. The data are from Ref. 12.

ment with the value of 120 meV obtained from a two-magnon light-scattering experiment.[13]

Here we present the results of a more extensive study of spin-wave dispersions in antiferromagnetic $YBa_2Cu_3O_{6+x}$. Most of the discussion will focus on measurements of our largest crystal, for which $x\sim0.3$ and $T_N=260$ K. To our surprise, we found the coupling between nearest-neighbor planes to be quite significant, although it is still probably much weaker than the in-plane exchange. The interaction between atoms in next-nearest-neighbor planes is much weaker than the bilayer coupling. A small anisotropy, probably due to spin-orbit coupling, results in a gap for out-of-plane spin-wave modes, making the layers weakly XY-like.

Because of their strong coupling, the two planes within a bilayer remain correlated well above T_N. Three-dimensional ordering occurs when the already well-correlated bilayers couple together along the c axis. The magnetic Bragg peak intensities saturated at low temperature in the two $x\sim0.15$ crystals studied; however, in the $x\sim0.3$ sample the Bragg peak intensities started to decrease as the temperature was decreased below 30 K. While the peaks at $(\frac{1}{2},\frac{1}{2},L+\frac{1}{2})$ reported by Kadowaki *et al.*[14] were not observed, we did find extra diffuse scattering along the $(\frac{1}{2},\frac{1}{2},l)$ rod, with the scattering peaked about the integral-l positions. Similar behavior has been reported by Rossat-Mignod and co-workers.[4] Low-energy inelastic magnetic scattering is enhanced at temperatures in the region of the transition. These observations can be explained in terms of an incoherent ordering of magnetic moments in the oxygen-deficient layers at low temperatures.

We have also looked for magnetic scattering in several superconducting crystals. Measurements[15–17] of the magnetic susceptibility as a function of oxygen content indicate that the magnetic properties of $YBa_2Cu_3O_{6+x}$ vary smoothly through the tetragonal-orthorhombic phase boundary and into the superconducting regime. However, we have not been successful in observing any low-energy ($\lesssim10$ meV) magnetic excitations. The most that we can say at this point is that the presence of mobile holes causes a significant modification of the cross section for low-energy excitations.

In order to understand the spin-wave measurements it is helpful to have a model with which to interpret them. Thus, we begin the paper by discussing a simple Heisenberg Hamiltonian for the magnetic Cu lattice and its spin-wave eigenmodes. After descriptions of the experimental procedure and sample characterization, scattering results for the $x\sim0.3$ antiferromagnetic crystal are presented and analyzed in terms of the spin-wave model. Next, the temperature dependence of the scattering is discussed. Finally, the measurements of the superconducting crystals are described. The paper concludes with a summary of our results.

II. SPIN-WAVE MODEL

A. Qualitative discussion

We expect that the dominant spin-spin interactions should occur between nearest-neighbor (NN) copper atoms and should have the Heisenberg form $J\mathbf{S}_i\cdot\mathbf{S}_j$. In-

teractions between the three different types of NN pairs must be considered. The strongest occurs due to superexchange within a plane, and the corresponding exchange constant will be designated as $J_{\parallel}$. We know from previous spin-wave dispersion measurements[12] and Raman studies[18] of $YBa_2Cu_3O_{6+x}$ that $J_{\parallel} \sim 100$ meV.

The CuO_2 planes are grouped in bilayers, with the two planes of a bilayer separated by a layer of Y atoms. Neighboring Cu atoms in different planes of a bilayer are separated by a distance $zc \approx 3.3$ Å, with no intervening atoms. Although superexchange between such a pair is not possible, direct exchange is. There is only one hole spin on each copper with the hole having $d_{x^2-y^2}$ symmetry. In such a case direct exchange is expected to yield an antiferromagnetic coupling[19] as is observed experimentally,[3] and we designate the exchange constant as $J_{\perp 1}$. The magnitude of $J_{\perp 1}$ can be estimated from calculations by Freeman and Watson[20] of direct exchange between Co atoms each having a $3d^9$ configuration. For two Co atoms separated by 2.4 Å along the z axis with a $d_{x^2-y^2}$ hole on each site, they obtained an exchange constant $J_{\delta\delta}=6$ meV. Some people have suggested that fluctuations of the Cu $3d$ hole into a $d_{3z^2-r^2}$ state could be important. For a pair of cobalt atoms with a $d_{3z^2-r^2}$ hole on each site, a value of $J_{\sigma\sigma} \approx 10 J_{\delta\delta}$ was found, and for mixed states $J_{\sigma\delta}=0$. The separation between Cu atoms in $YBa_2Cu_3O_{6+x}$ is certainly much greater than the value used in the calculations, so that a significant reduction in the exchange constant $J_{\perp 1}$ relative to the calculated values is expected. Nevertheless, it appears that direct exchange could result in $J_{\perp 1} \sim 1$ meV. If we write $\alpha_{\perp 1}=J_{\perp 1}/J_{\parallel}$, then $\alpha_{\perp 1} \sim 10^{-2}$.

A pair of bilayers is separated by a CuO_x "chain" layer. A Cu site in an oxygen-deficient layer is commonly labeled Cu(1), while a site in a CuO_2 plane is denoted by Cu(2). A Cu(2) atom is connected to the nearest Cu(2) in the next bilayer by an O-Cu(1)-O bridge. A study[21] using x-ray absorption spectroscopy has demonstrated that essentially all of the Cu(1) atoms have a nonmagnetic $3d^{10}$ configuration in $YBa_2Cu_3O_6$. The magnetic interaction between $Cu(2)^{2+}$ atoms in neighboring bilayers probably occurs through some high-order superexchange process via the intervening O-$Cu(1)^{1+}$-O bridge. With increasing oxygen content, some of the $Cu(1)^{1+}$ are converted to magnetic $Cu(1)^{2+}$. The $3d$ hole on a $Cu(1)^{2+}$ has $d_{y^2-z^2}$ symmetry. Because this hole is orthogonal to the $d_{x^2-y^2}$ holes in the planes, the superexchange coupling between chain and plane nearest neighbors should be ferromagnetic.[22,23] In the magnetic structure observed in samples with small x,[3] the planar Cu^{2+} spins are oriented antiferromagnetically along the c axis, so that the net coupling to a magnetic Cu(1) would be zero (assuming classical spins and perfect Néel order). If we label the net exchange constant between planar Cu atoms in neighboring bilayers as $J_{\perp 2}$, then we expect $\alpha_{\perp 2}=J_{\perp 2}/J_{\parallel} \ll 1$. With increasing x, the frustrated couplings result in a net decrease of $J_{\perp 2}$ which contributes to the observed decrease in T_N.[3,4]

In our inelastic scattering measurements we have observed an energy gap for spin-wave modes involving spin deviations out of the CuO_2 planes, and no gap for in-plane modes. To model this anisotropy, a small anisotropic exchange term must be included in the spin Hamiltonian. Such a term can result from spin-orbit coupling.[24,25] The simplest anisotropic term appropriate for a spin-$\frac{1}{2}$ system with XY symmetry has the form $-DS_i^zS_j^z$. The anisotropy parameter D can be calculated with third-order perturbation theory,[24,25] and its magnitude should be comparable to $J(g-2)^2$. This expression is probably an upper limit, as experimental values can be much smaller than such a crude estimate.[26] Since $J_{\parallel}$ is the largest exchange constant in the problem and $(g-2)^2$ is small, it should be sufficient to include anisotropic exchange only between spins in the same plane. The g factor has not been measured in any of the layered cuprate compounds because electron spin resonance measurements have not revealed any intrinsic resonance feature in these systems. Nevertheless, if we assume a typical[27] value of $g \sim 2.1$, then we expect $\alpha_D = D/J_{\parallel} \lesssim 10^{-2}$.

B. The spin Hamiltonian and its solution

We will ignore Cu atoms in the chain sites and consider only those in the planes. Those Cu atoms form a tetragonal lattice with a two-atom basis consisting of one site in each of the two planes in a unit cell. Let $\mathbf{n}$ label the unit cells and let $\kappa = A, C$ label the two basis sites, as indicated in Fig. 1(a). The spin Hamiltonian can then be written as

$$H = \tfrac{1}{2}J_{\parallel}\sum_{\mathbf{n}\kappa\mathbf{a}}(\mathbf{S}_{\mathbf{n}\kappa}\cdot\mathbf{S}_{\mathbf{n}+\mathbf{a},\kappa} - \alpha_D S^z_{\mathbf{n}\kappa}S^z_{\mathbf{n}+\mathbf{a},\kappa}) + J_{\perp 1}\sum_{\mathbf{n}}\mathbf{S}_{\mathbf{n}A}\cdot\mathbf{S}_{\mathbf{n}+\mathbf{c},C} + J_{\perp 2}\sum_{\mathbf{n}}S_{\mathbf{n}A}\cdot\mathbf{S}_{\mathbf{n}C}\ , \quad (1)$$

where $\mathbf{a}$ denotes displacements to NN sites within a CuO_2 plane and $\mathbf{c}$ indicates a unit-cell displacement along the c axis. The magnetic lattice has a four-atom basis resulting from the basis of the chemical lattice and the two spin directions. In general, there will be four spin-wave modes. The chemical basis splits them into two acoustic and two optical modes (labeled by analogy with phonons), and the anisotropy splits each pair into in-plane and out-of-plane modes.

As the XY symmetry of the model Hamiltonian allows the spins to point in any direction in the plane, we will arbitrarily choose the spin directions to be parallel and antiparallel to the x axis. Let the two antiparallel spins in plane A of unit cell $\mathbf{n}$ be labeled $\mathbf{S}_{\mathbf{n}a}$ and $\mathbf{S}_{\mathbf{n}b}$. Following the standard approach,[28] we make the Holstein-Primakoff transformation to boson creation and destruction operators $a^\dagger_{\mathbf{n}}, a_{\mathbf{n}}, b^\dagger_{\mathbf{n}}, b_{\mathbf{n}}$:

$$\begin{aligned} &S^x_{\mathbf{n}a} = \tfrac{1}{2} - a^\dagger_{\mathbf{n}}a_{\mathbf{n}}, \quad S^x_{\mathbf{n}b} = -\tfrac{1}{2} + b^\dagger_{\mathbf{n}}b_{\mathbf{n}}\ , \\ &S^+_{\mathbf{n}a} = (1 - a^\dagger_{\mathbf{n}}a_{\mathbf{n}})^{1/2}a_{\mathbf{n}}, \quad S^+_{\mathbf{n}b} = b^\dagger_{\mathbf{n}}(1 - b^\dagger_{\mathbf{n}}b_{\mathbf{n}})^{1/2}\ , \\ &S^-_{\mathbf{n}a} = a^\dagger_{\mathbf{n}}(1 - a^\dagger_{\mathbf{n}}a_{\mathbf{n}})^{1/2}, \quad S^-_{\mathbf{n}b} = (1 - b^\dagger_{\mathbf{n}}b_{\mathbf{n}})^{1/2}b_{\mathbf{n}}\ , \end{aligned} \quad (2)$$

where $S^{\pm} = S^z \pm iS^y$. In the C layer, let the spin on site c sit above and be antiparallel to b in layer A. The trans-

formation for spin c has the same form as that for a, with $a_n^\dagger, a_n$ replaced by $c_n^\dagger, c_n$. Spin d sits above a and has the same transformation as b. Spin-wave operators are obtained by Fourier transforming to reciprocal space:

$$\begin{aligned} a_q &= N^{-1/2}\sum_n e^{iq\cdot n}a_n \ , \\ a_q^\dagger &= N^{-1/2}\sum_n e^{-iq\cdot n}a_n^\dagger \ , \\ b_q &= N^{-1/2}\sum_n e^{-iq\cdot(n+a)}b_n \ , \\ b_q^\dagger &= N^{-1/2}\sum_n e^{iq\cdot(n+a)}b_n^\dagger \ , \end{aligned} \tag{3}$$

etc., where N is the number of magnetic unit cells in the crystal. Applying these transformations to Eq. (1) and retaining only those terms which are bilinear in the spin-wave operators (the usual linear-spin-wave approximation), one obtains the approximate Hamiltonian

$$\begin{aligned} \frac{H_0}{\hbar\omega_\parallel} = \sum_q \{ &(1+\tfrac{1}{4}\alpha_\perp)(a_q^\dagger a_q + b_q^\dagger b_q + c_q^\dagger c_q + d_q^\dagger d_q) \\ &+\gamma_\parallel(1-\tfrac{1}{2}\alpha_D)(a_q b_q + a_q^\dagger b_q^\dagger + c_q d_q + c_q^\dagger d_q^\dagger) \\ &+\tfrac{1}{4}\alpha_\perp[\gamma_\perp(a_q d_q + b_q^\dagger c_q^\dagger)+\gamma_\perp^*(a_q^\dagger d_q^\dagger + b_q c_q)] \\ &-\tfrac{1}{2}\alpha_D\gamma_\parallel(a_q b_{-q}^\dagger + a_q^\dagger b_{-q} + c_q d_{-q}^\dagger + c_q^\dagger d_{-q})\} \ , \end{aligned} \tag{4}$$

where

$$\hbar\omega_\parallel = 2J_\parallel \ , \tag{5}$$

$$\alpha_\perp = \alpha_{\perp 1} + \alpha_{\perp 2} \ , \tag{6}$$

$$\gamma_\parallel = \tfrac{1}{2}[\cos(q_x a)+\cos(q_y a)] \ , \tag{7}$$

and

$$\gamma_\perp = |\gamma_\perp| e^{i\phi_\perp} \ , \tag{8}$$

with

$$|\gamma_\perp| = \frac{[J_{\perp 1}^2 + J_{\perp 2}^2 + 2J_{\perp 1}J_{\perp 2}\cos(q_z c)]^{1/2}}{(J_{\perp 1}+J_{\perp 2})} \ , \tag{9}$$

$$\phi_\perp = \tan^{-1}\left[\frac{J_{\perp 1}\sin(q_z zc) - J_{\perp 2}\sin[q_z(1-z)c]}{J_{\perp 1}\cos(q_z zc) + J_{\perp 2}\cos[q_z(1-z)c]}\right] . \tag{10}$$

The Hamiltonian H_0 can be diagonalized by making a Bogoliubov-type transformation. The eigenfrequencies ω_{qj} are given by

$$\left(\frac{\omega_{qj}}{\omega_\parallel}\right)^2 = (1+\tfrac{1}{4}\alpha_\perp \mp \tfrac{1}{2}\alpha_D\gamma_\parallel)^2 - (\gamma_\parallel \pm \tfrac{1}{4}\alpha_\perp|\gamma_\perp| - \tfrac{1}{2}\alpha_D\gamma_\parallel)^2 \ , \tag{11}$$

where the eigenmode labels $j=1$, 2, 3, and 4 correspond to the sign combinations $-+$, $++$, $--$, and $+-$, respectively, in Eq. (11). The modes $j=1$ and 3 are the in-plane acoustic and optical modes, respectively, while $j=2$ and 4 denote the out-of-plane acoustic and optical modes. The eigenoperators are

$$\begin{aligned} \alpha_{q1} &= u_{q1}^*(a_q + b_{-q}) + u_{q1}(c_q + d_{-q}) \\ &\quad - v_{q1}^*(a_{-q}^\dagger + b_q^\dagger) - v_{q1}(c_{-q}^\dagger + d_q^\dagger) \ , \\ \beta_{q2}^\dagger &= -v_{q2}^*(a_q - b_{-q}) - v_{q2}(c_q - d_{-q}) \\ &\quad - u_{q2}^*(a_{-q}^\dagger - b_q^\dagger) - u_{q2}(c_{-q}^\dagger - d_q^\dagger) \ , \\ \alpha_{q3} &= u_{q3}^*(a_q + b_{-q}) - u_{q3}(c_q + d_{-q}) \\ &\quad - v_{q3}^*(a_{-q}^\dagger - b_q^\dagger) + v_{q3}(c_{-q}^\dagger + d_q^\dagger) \ , \\ \beta_{q4}^\dagger &= -v_{q4}^*(a_q - b_{-q}) + v_{q4}(c_q - d_{-q}) \\ &\quad - u_{q4}^*(a_{-q}^\dagger - b_q^\dagger) + u_{q4}(c_{-q}^\dagger - d_q^\dagger) \ , \end{aligned} \tag{12}$$

where for $j=1$, 3, the coefficients u_{qj} and v_{qj} are given by

$$\begin{aligned} u_{qj} &= \left[\frac{1+\frac{1}{4}\alpha_D - \frac{1}{2}\alpha_D\gamma_\parallel + \omega_{qj}}{8\omega_{qj}}\right]^{1/2} e^{i\phi_\perp/2} \ , \\ v_{qj} &= \left[\frac{1+\frac{1}{4}\alpha_D - \frac{1}{2}\alpha_D\gamma_\parallel - \omega_{qj}}{8\omega_{qj}}\right]^{1/2} e^{i\phi_\perp/2} \ , \end{aligned} \tag{13}$$

and for $j=2$, 4,

$$\begin{aligned} u_{qj} &= \left[\frac{1+\frac{1}{4}\alpha_D + \frac{1}{2}\alpha_D\gamma_\parallel + \omega_{qj}}{8\omega_{qj}}\right]^{1/2} e^{i\phi_\perp/2} \ , \\ v_{qj} &= \left[\frac{1+\frac{1}{4}\alpha_D + \frac{1}{2}\alpha_D\gamma_\parallel - \omega_{qj}}{8\omega_{qj}}\right]^{1/2} e^{i\phi_\perp/2} \ . \end{aligned} \tag{14}$$

Our measurements are restricted to relatively low energies, and because of the large spin-wave dispersion we can only study magnons with small $\mathbf{q}_\parallel$. Taking into account that $\alpha_\perp, \alpha_D \ll 1$ and setting $\mathbf{q}_\parallel = (q_\parallel, q_\parallel, 0)/\sqrt{2}$ Eq. (11) can be expanded to give

$$\begin{aligned} \omega_{q1} &\approx \frac{\omega_\parallel}{\sqrt{2}}[q_\parallel^2 a^2 + \alpha_\perp(1-|\gamma_\perp|)]^{1/2} \ , \\ \omega_{q2} &\approx \frac{\omega_\parallel}{\sqrt{2}}[q_\parallel^2 a^2 + \alpha_\perp(1-|\gamma_\perp|) + 4\alpha_D]^{1/2} \ , \\ \omega_{q3} &\approx \frac{\omega_\parallel}{\sqrt{2}}[q_\parallel^2 a^2 + \alpha_\perp(1+|\gamma_\perp|)]^{1/2} \ , \\ \omega_{q4} &\approx \frac{\omega_\parallel}{\sqrt{2}}[q_\parallel^2 a^2 + \alpha_\perp(1+|\gamma_\perp|) + 4\alpha_D]^{1/2} \ . \end{aligned} \tag{15}$$

If we set $\mathbf{q}_\parallel = 0$, then the frequencies at the Brillouin zone center and zone boundary ($q_z = 0$ and $q_z = \pi/c$, respectively) have particularly simple expressions, as shown in Table I. Although the frequencies listed in the table are proportional to small parameters, they are also proportional to the very large quantity $\omega_\parallel$, so that the dispersion of the acoustic mode along q_z and the gaps between modes can be substantial. As an example, Fig. 3 shows dispersion curves along the [110] direction, in the CuO_2 plane, and along [001], perpendicular to the plane, calculated with the parameters $J_\parallel = 100$ meV, $\alpha_{\perp 1} = 0.026$, $\alpha_{\perp 2} = 2.6\times10^{-4}$, and $\alpha_D = 3.4\times10^{-4}$. The parameters $\alpha_{\perp 1}$, $\alpha_{\perp 2}$, and α_D can in principal be determined by

TABLE I. Zone-center and zone-boundary spin-wave frequencies (normalized to $\omega_{\parallel}$) calculated using Eq. (11) with $\alpha_{\perp 1} > \alpha_{\perp 2}$.

Mode j	Zone Center $q_{\parallel}=0,\ q_z=0$	Zone Boundary $q_{\parallel}=0,\ q_z=\pi/c$
1	0	$\sqrt{\alpha_{\perp 2}}$
2	$\sqrt{\alpha_D}$	$\sqrt{\alpha_{\perp 2}+\alpha_D}$
3	$\sqrt{\alpha_{\perp}}$	$\sqrt{\alpha_{\perp 1}}$
4	$\sqrt{\alpha_{\perp}+\alpha_D}$	$\sqrt{\alpha_{\perp 1}+\alpha_D}$

measuring the spin-wave frequencies at zone center and zone boundary. The value of $J_{\parallel}$ can be obtained near zone center from the 2D spin-wave velocity ($c=\omega_{q_{\parallel}1}/q_{\parallel}$) for the acoustic, in-plane mode, which is equal to $\sqrt{2}J_{\parallel}a$.

C. Scattering cross section

The differential scattering cross section for spin waves in $YBa_2Cu_3O_{6+x}$ can be written[29]

$$\frac{d^2\sigma}{d\Omega_f dE_f}=\frac{N}{\hbar}\left[\frac{\gamma e^2}{m_e c^2}\right]^2\frac{k_f}{k_i}[\tfrac{1}{2}gf(\mathbf{Q})e^{-W(\mathbf{Q})}]^2 \times[\tfrac{1}{2}(1+\hat{Q}_z^{\,2})\mathcal{S}^{yy}(\mathbf{Q},\omega) +(1-\hat{Q}_z^{\,2})\mathcal{S}^{zz}(\mathbf{Q},\omega)]\ , \tag{16}$$

where γ is the gyromagnetic ratio of the neutron, $f(\mathbf{Q})$ is the magnetic form factor for a Cu atom, $\exp[-W(\mathbf{Q})]$ is a Debye-Waller factor, and $\hat{Q}_z=Q_z/Q$. The scattering function $\mathcal{S}^{\alpha\alpha}(\mathbf{Q},\omega)$ can be calculated using the general formula

$$\mathcal{S}^{\alpha\alpha}(\mathbf{Q},\omega)=\frac{1}{2\pi}\sum_{\mathbf{n}}\int_{-\infty}^{\infty}e^{i(\mathbf{Q}\cdot\mathbf{n}-\omega t)}\langle S_0^{\alpha}(0)S_{\mathbf{n}}^{\alpha}(t)\rangle dt\ . \tag{17}$$

Applying the results of the previous section, we find that for the creation of spin waves

$$\mathcal{S}^{yy}(\mathbf{Q},\omega)=\sum_{\mathbf{G}}\delta(\mathbf{Q}-\mathbf{q}-\mathbf{G}) \times\sum_{j=1,3}(n_{\mathbf{q}j}+1)\delta(\hbar\omega-\hbar\omega_{\mathbf{q}j}) \times(|u_j|-|v_j|)^2 g^2(\mathbf{q},j)\ , \tag{18}$$

where we have restricted the sum on $\mathbf{G}$ to allowed antiferromagnetic (AF) Bragg peak positions, and we have dropped the neglible terms in which $\mathbf{G}$ is a reciprocal lattice vector of the chemical lattice. The formula for $\mathcal{S}^{zz}(\mathbf{Q},\omega)$ is exactly the same as Eq. (18) except that the sum over modes covers $j=2,4$ instead of $j=1,3$. The Bose factor

$$n_{\mathbf{q}j}=[\exp(\hbar\omega_{\mathbf{q}j}/kT)-1]^{-1}\ ,$$

and the magnetic structure factor $g(\mathbf{q},j)$ is given by

$$g(\mathbf{q},j)=\begin{cases}\sin[\frac{1}{2}(\mathbf{G}\cdot\boldsymbol{\rho}-\phi_{\perp})] & \text{for } j=1,2;\\ \cos[\frac{1}{2}(\mathbf{G}\cdot\boldsymbol{\rho}-\phi_{\perp})] & \text{for } j=3,4,\end{cases} \tag{19}$$

where $\boldsymbol{\rho}=z\mathbf{c}$ points between nearest-neighbor CuO_2 planes. Using Eqs. (13) and (14), it is easy to show that for $q_{\parallel}a,\alpha_{\perp},\alpha_D \ll 1$,

$$(|u_{\mathbf{q}j}|-|v_{\mathbf{q}j}|)^2\approx\frac{1}{2\omega_{\mathbf{q}j}}\ . \tag{20}$$

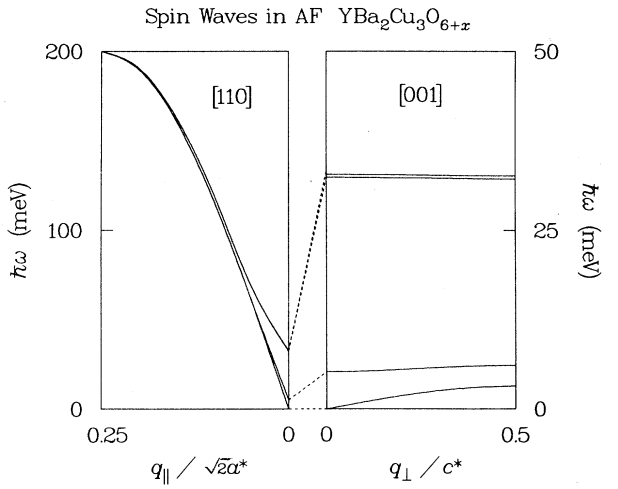

FIG. 3. Schematic diagram of spin-wave dispersion in $YBa_2Cu_3O_{6+x}$ calculated from Eq. (11) with $J_{\parallel}=100$ meV, $J_{\perp 1}=2.6$ meV, $J_{\perp 2}=0.026$ meV, and $D=0.034$ meV. Note that the energy scales for the two panels differ by a factor of 4. The 2D nature of the magnetic interactions makes the dispersion very large along $q_{\parallel}$ but extremely weak along $q_{\perp}$.

III. EXPERIMENTAL DETAILS

A. Neutron scattering

The unpolarized neutron scattering measurements were performed on triple-axis spectrometers H4M, H7, and H9A at the High Flux Beam Reactor located at Brookhaven National Laboratory. Pyrolytic graphite (002) reflections were used for the monochromator and analyzer, with typical horizontal collimations of 40′-40′-40′-80′. At H4M and H7 the analyzer was fixed at 14.7 meV, and a pyrolytic graphite filter was used to eliminate neutrons with a wavelength of $\lambda/2$. For measurements at H9A the incident energy was fixed at 5.0 meV and a Be filter was employed to eliminate harmonics.

Each crystal was wrapped in Al foil and mounted on a thin Al disk. The mount was enclosed in an Al can filled with He gas for heat-exchange purposes. For measurements from 5 to 350 K, the sample can was usually mounted in a cryostat cooled with liquid N_2 or He and having a thermal weak link allowing temperature adjustment with a heating resistor. In some cases a Displex

closed-cycle refrigerator was used. Temperatures were measured with either a Ge diode or a Pt resistance thermometer. One crystal was heated to 500 K in a furnace with a stagnant He atmosphere.

Measurements using polarized neutrons with polarization analysis were performed on triple-axis spectrometer H8. The technique has been described in detail elsewhere.[30] Briefly, the spectrometer is set up so as to measure spin-flip (magnetic) scattering. Measurements are made with a magnetic guide field applied to the sample, with the field first parallel (horizontal) and then perpendicular (vertical) to the scattering vector. By taking the difference between the horizontal field (HF) and vertical field (VF) intensities, one obtains a signal proportional to one-half of the magnetic cross section, with the background and residual nuclear scattering contributions in each channel canceling. For the inelastic scattering measurements, the final neutron energy was 41 meV and no filter was used.

Superconducting transition temperatures were determined by the neutron depolarization technique.[31] This method is bulk sensitive, and it is practical for samples which are too large to fit in a conventional magnetometer. The H8 spectrometer was first positioned at a strong nuclear Bragg peak of the sample, and the neutron spin flipper was then adjusted so that only spin-flip scattering would be detected. (Because of the finite polarization sensitivity of the spectrometer a small background non-spin-flip signal was always observed along with the spin-incoherent scattering.) For each data point, the sample was cooled from above T_c in a vertical guide field. When the measurement temperature was reached, the scattered signal was first measured with the vertical field applied. The guide field at the sample was then changed to the horizontal direction, and a second measurement of the scattered signal was made. In the normal state the VF and HF signals were equally small; however, in the superconducting state, flux trapped in the sample during cooling in the vertical field causes the polarization of the scattered beam to be rotated nonadiabatically when the horizontal field is applied. Thus, a large increase in the HF spin-flip signal is observed when the sample is cooled below T_c. While this technique provides a good measure of the transition temperature and its sharpness, we do not understand the depolarization process well enough to be able to estimate the fraction of the sample that is superconducting.

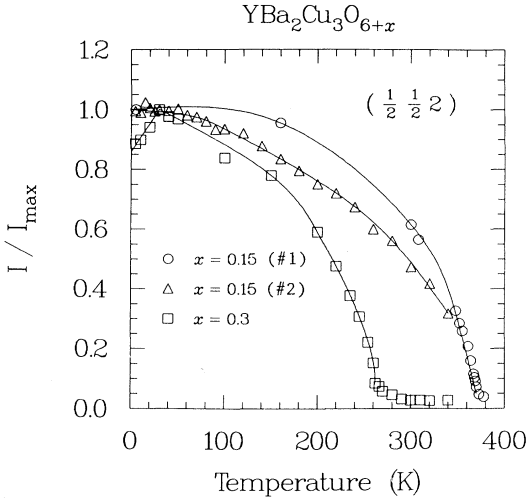

FIG. 4. Peak intensity of the $(\frac{1}{2},\frac{1}{2},2)$ antiferromagnetic Bragg peak in three $YBa_2Cu_3O_{6+x}$ single crystals as a function of temperature. The solid lines are guides to the eye.

B. Crystal growth and characterization

The $YBa_2Cu_3O_{6+x}$ crystals were grown and treated at the Institute for Molecular Science; the details have been described elsewhere.[32] To obtain large crystals it was necessary to start with a mixture rich in Ba and Cu. "Ingot crystals" of nearly 1 cm^3 have been grown which include significant amounts of the solidified non-stoichiometric flux. A single ingot can contain $YBa_2Cu_3O_{6+x}$ crystals with different orientations as well as polycrystalline $BaCuO_2$ impurities. The best samples (the ones which we have chosen to study) contain a large fraction of uniquely oriented $YBa_2Cu_3O_{6+x}$ crystal blocks with a mosaic spread of $\lesssim 2°$.

Each crystal was characterized with several different neutron scattering measurements, the results of which are summarized in Table II. The relative scattering volumes were determined by comparing the intensity observed for an acoustic phonon at $\mathbf{Q}=(0,0,6.3)$ and from spin-wave intensities for the antiferromagnetic crystals. From various observations we estimate the scattering volume of crystal 3 to be approximately 0.5 cm^3. The lattice parameters listed were measured at 300 K. The c lattice param-

TABLE II. Various properties of the $YBa_2Cu_3O_{6+x}$ single crystals studied by neutron scattering. The scattering volume V has an uncertainty of 50%. The estimated uncertainty in x is ± 0.1.

x	Crystal No.	V (cm^3)	Mosaic (FWHM)	$\frac{1}{2}(a+b)$ (Å)	c (Å)	M (μ_B)	T_N (K)	T_c (K)
0.15	1	0.1	1.2°	3.863	11.82	0.35±0.05	370±5	
0.15	2	0.1	1.6°	3.865	11.82	0.34±0.05	>340	
0.3	3	0.5	1.8°	3.863	11.80	0.36±0.05	260±5	
0.45	4	0.1	2.8°	3.862	11.75			40±5
0.5	5	0.1	1.5°	3.863	11.73			20±10
0.8	6	0.1	2.3°	3.858	11.70			83±10
0.9	7	0.3	2.4°	3.860	11.70			85±5

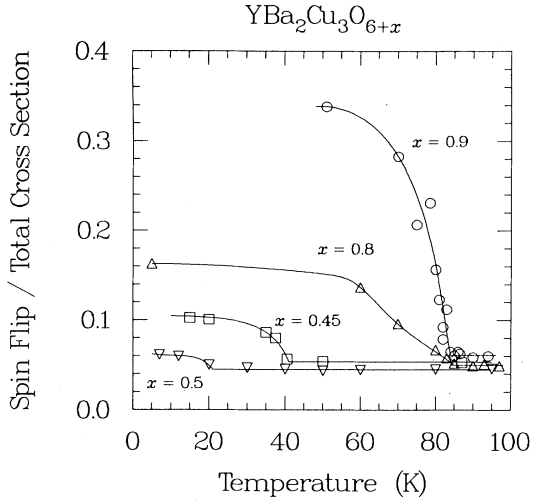

FIG. 5. Ratio of the spin-flip scattering to the total scattered intensity from a Bragg peak due to depolarization of an initially polarized neutron beam, as discussed in the text. The initial rise in the spin-flip signal indicates the onset of superconductivity. The solid lies are guides to the eye.

eter was used to estimate the oxygen content x by comparison with data for c versus x found in the literature.[33] The Néel temperatures were determined from the temperature dependence of the $(\frac{1}{2},\frac{1}{2},2)$ antiferromagnetic Bragg peak as illustrated in Fig. 4. The relatively sharp transitions indicate that the crystals were reasonably homogeneous. The low-temperature-ordered magnetic moment M for each crystal was obtained by comparing the intensities of four magnetic peaks with those of 5–7 nuclear reflections. Extinction was a problem for the stronger nuclear peaks, and an empirical correction was made for it; however, because of the unsymmetrical

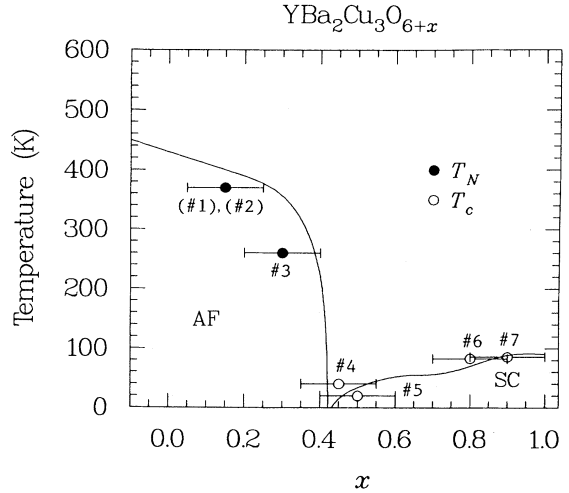

FIG. 6. Temperature vs oxygen content phase diagram for $YBa_2Cu_3O_{6+x}$ from Ref. 3. The symbols represent the single crystals studied in the present work. AF and SC stand for antiferromagnetic and superconducting, respectively.

shapes of the crystals and the small number of reflections used, a large systematic error is possible. The depolarization measurements used to determine T_c in the superconducting crystals are shown in Fig. 5. The depolarization signal was quite large for crystal 7, which also had the highest T_c. The transition temperatures (both magnetic and superconducting) as a function of x are compared in Fig. 6 with the phase diagram previously determined.[3]

IV. SPIN-WAVE MEASUREMENTS AND ANALYSIS

A. Fitting analysis

In order to extract exchange parameters from our spin-wave measurements it is necessary to fit the data by convolving the theoretical scattering cross section with the calculated spectrometer resolution function. At finite temperatures the sharp spin-wave excitations broaden in energy due to magnon-magnon interactions, and for that reason, as well as for numerical reasons, the δ function in Eq. (18) is usually replaced by a Lorentzian with a half-width Γ. In fitting some of the constant-Q scans it was found that to get agreement with the measurements it was necessary to use a value of Γ much less than the energy resolution. As this caused problems in the numerical evaluation of the convolution integral, a new convolution routine was written which assumes that the spin-wave cross section does indeed contain a δ function in energy. All of the fits shown in this paper were performed assuming sharp excitations. They were made taking into account both the in-plane and out-of-plane acoustic modes with the experimentally determined exchange parameters discussed below. For each scan a scale factor was included in the calculations in order to fit the amplitude of the data. For the constant-ΔE scans, constant and linear background terms were also included.

In a typical scattering measurement, the neutron flux coming from the monochromator is monitored, and the scattered intensity is measured for a fixed number of monitor counts. When the final energy is held fixed during a scan, the filter is placed after the sample to eliminate neutrons at the second harmonic energy. However, the higher-order neutrons are still detected by the monitor, and since the harmonic content of the beam varies with energy, a fixed monitor count does not correspond to a fixed number of incident neutrons of the desired energy. The harmonic content has been measured as a function of energy,[34] thus making it possible to correct the data for contamination of the monitor signal. The correction has been applied to all data shown in this paper where intensity as a function of energy transfer is important. For a fixed final energy of 14.7 meV, the correction for an energy transfer $\Delta E=10$ meV relative to $\Delta E=2$ meV is a 30% reduction in intensity.

B. Results

As discussed in the Introduction, the spin-wave dispersion in antiferromagnetic $YBa_2Cu_3O_{6+x}$ is nearly two dimensional. Figure 7 shows scans across the 2D scattering rod [scan type A in Fig. 1(b)] at the magnetic Bragg

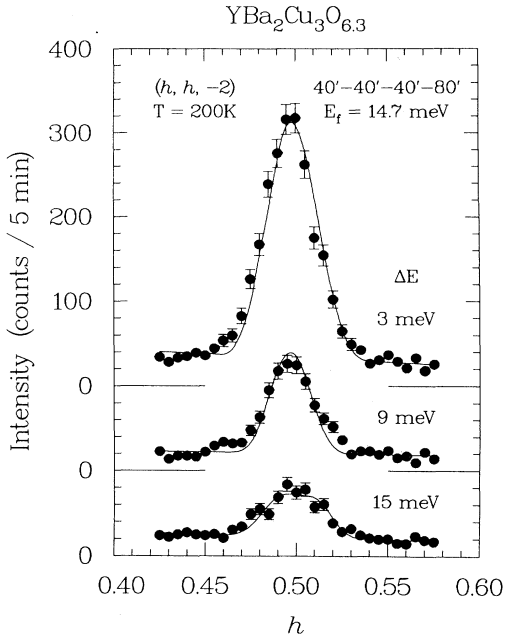

FIG. 7. Several constant ΔE scans across the 2D magnetic ridge in $YBa_2Cu_3O_{6.3}$ (crystal 3) at 200 K. The intensities have been adjusted slightly as noted in the caption for Fig. 2. The solid lines are fits which are discussed in the text.

peak position $(\frac{1}{2},\frac{1}{2},-2)$ [$\mathbf{q}=(0,0,0)$] for energy transfers of 3, 9, and 15 meV. The measurements were performed on crystal 3 ($x\approx 0.3$) at 200 K; the solid lines are fits to the data. From the 15-meV scan, we obtain an in-plane exchange constant of $J_{\parallel}=80^{+60}_{-30}$ meV. Confirmation of the magnetic nature of these excitations is given by the polarized beam data shown in Fig. 8.

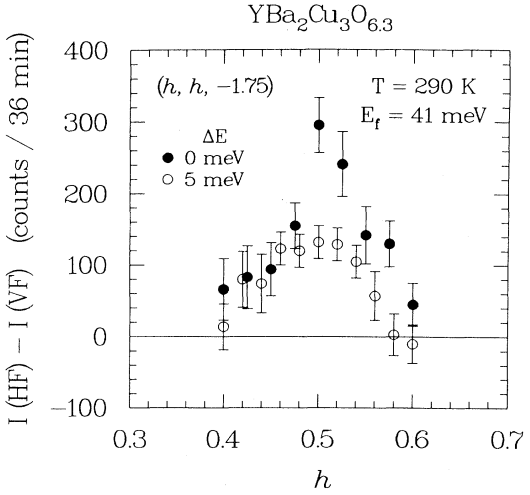

FIG. 8. Constant ΔE scans at 290 K in $YBa_2Cu_3O_{6.3}$ confirming the magnetic nature of the inelastic 2D scattering. Measurements were performed with polarized neutrons. The abscissa corresponds to the difference in spin-flip scattering for horizontal and vertical field conditions, as discussed in the text. The energy resolution for these measurements was approximately 9 meV.

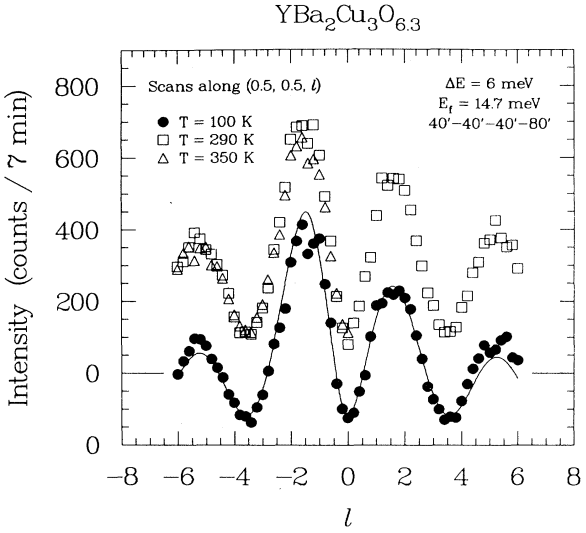

FIG. 9. Constant ΔE scan of type B (see Fig. 1) along the 2D rod with $\Delta E=6$ meV. The modulation is due to the inelastic structure factor $g^2(\mathbf{q},j)$. The enhancement near $l=-1.5$ is due to a "focusing" effect of the spectrometer resolution function. The solid line is a fit which is discussed in the text.

Figure 9 shows scans along the $(\frac{1}{2},\frac{1}{2},l)$ rod for $\Delta E=\hbar\omega=6$ meV at temperatures both above and below T_N. The dominant contribution to the modulation is from the acoustic mode structure factor, which is described by Eqs. (19) and (10). For $J_{\perp 1}\gg J_{\perp 2}$, the phase factor $\phi_\perp$ can be approximated by

$$\phi_\perp \approx 2\pi z l-(J_{\perp 2}/J_{\perp 1})\sin(2\pi l)\ , \tag{21}$$

where z, the relative separation between NN planes, is equal to 0.28 (Ref. 33). Assuming that the second term makes a negligible contribution, Eqs. (19) and (21) predict minima at $l=n/z=0$, ± 3.6, ± 7.1, etc., as observed. The solid line is a calculation for $T=200$ K using our spin-wave model. The good agreement with the data is somewhat fortuitous since the magnetic form factor for copper was not included in the calculation. (The Q dependence of the form factor is important only for scans over a wide Q range.) However, the calculation is sensitive to the mosaic of the sample, which has been crudely approximated by a Gaussian, so that discrepancies are to be expected.

That $J_{\perp 1}$ is much greater than $J_{\perp 2}$ is consistent with the fact that we observe only the acoustic mode modulation at low energies. From Eqs. (18) and (20) we see that at a given energy the acoustic and optical modes should have the same cross section (if we ignore the structure factors). Since the structure factors for the acoustic and optical modes are 180° out of phase, the modulation would disappear if both were present at the same energy ($\sin^2\phi+\cos^2\phi=1$). To search for the in-plane optical mode, we moved the spectrometer to a minimum of the acoustic structure factor, $\mathbf{Q}=(\frac{1}{2},\frac{1}{2},-3.6)$, and scanned the energy transfer up to 30 meV. For comparison we also scanned at an acoustic mode peak $(\frac{1}{2},\frac{1}{2},-5.4)$. The results are shown in Fig. 10, with the background signal

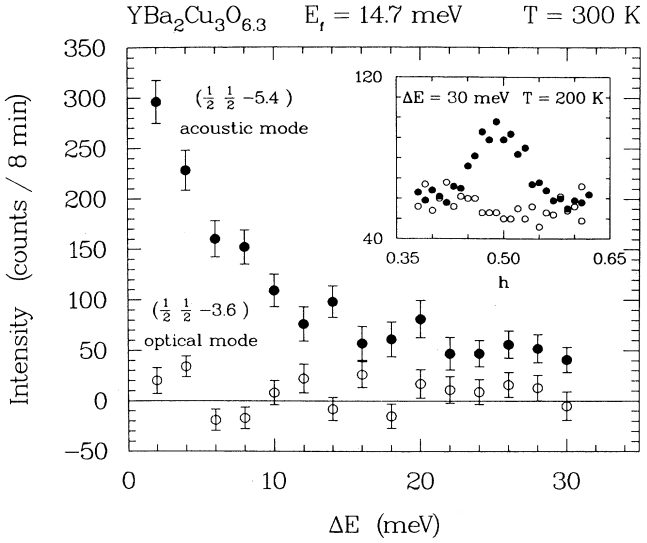

FIG. 10. Scans as a function of energy transfer at two different points along the 2D rod, with the background signal (measured off of the rod) subtracted. The solid circles were measured at $\mathbf{Q}=(\frac{1}{2},\frac{1}{2},-5.4)$ where the structure factor for the acoustic mode is at a maximum, while the open circles correspond to $\mathbf{Q}=(\frac{1}{2},\frac{1}{2},-3.6)$ where the optical-mode structure factor should have a maximum. The inset shows scans across the 2D rod at the two different l points with $\Delta E=30$ meV and no background correction. The lack of signal at $l=-3.6$ indicates that the minimum optical-mode energy must be greater than 30 meV.

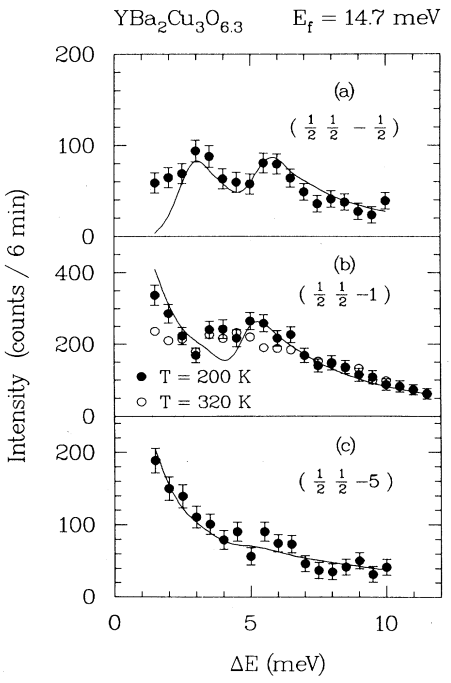

FIG. 11. Constant-Q scans at several points along the 2D rod to demonstrate the polarization dependence of the in- and out-of-plane acoustic modes. (a) $\mathbf{Q}=(\frac{1}{2},\frac{1}{2},-\frac{1}{2})$, $\mathbf{q}=(0,0,-\frac{1}{2})$. (b) $\mathbf{Q}=(\frac{1}{2},\frac{1}{2},-1)$, $\mathbf{q}=(0,0,0)$. (c) $\mathbf{Q}=(\frac{1}{2},\frac{1}{2},-5)$, $\mathbf{q}=(0,0,0)$. The solid lines are fits which are discussed in the text.

[measured at $(\frac{1}{2}\pm\delta,\frac{1}{2}\pm\delta,l)$ with $\delta=0.05$] subtracted off. The inset shows scans across the 2D rod at the two Q points for $\Delta E=30$ meV. The acoustic mode signal is still clearly present at 30 meV, but there is no sign of an optical mode. From this measurement, we obtain a lower limit for $J_{\perp 1}$ of 2 meV.

The next problem is to determine the out-of-plane anisotropy gap and the acoustic mode dispersion. To do this we have moved to zone-boundary and zone-center positions for small l (where both in-plane and out-of-plane modes should be strong) and scanned the energy. Panels (a) and (b) of Fig. 11 show such scans at $\mathbf{Q}=(\frac{1}{2},\frac{1}{2},-\frac{1}{2})$ and $(\frac{1}{2},\frac{1}{2},-1)$, respectively. For $\mathbf{Q}=(\frac{1}{2},\frac{1}{2},-1)$ (zone center) we find a peak at ~ 5 meV due to the out-of-plane mode, while at $(\frac{1}{2},\frac{1}{2},-\frac{1}{2})$ we see peaks at ~ 3 meV and ~ 6 meV, corresponding to zone boundary in-plane and out-of-plane modes, respectively. The fitted curves shown in the figure were calculated with $J_{\perp 2}=0.020$ meV (assuming $J_{\parallel}=80$ meV) and $D=0.035$ meV ($\alpha_D=4.4\times10^{-4}$). The uncertainties in these values are approximately ± 0.005 meV. Moving to large l, we find that the out-of-plane mode is greatly reduced in intensity as expected from its polarization dependence.

We have observed no evidence of a gap in the in-plane acoustic mode down to $\hbar\omega\sim 1.5$ meV. In order to test for a gap at lower energies, we improved the energy resolution by using incident neutrons with an energy of 5 meV. Unfortunately, most of the measurements were performed at 100 K where excess low-energy scattering is observed due to moments on the Cu(1) sites, as discussed in the next section. Further work is required to determine whether a finite gap exists in the in-plane mode.

Figure 12 shows a scan along the $(\frac{1}{2},\frac{1}{2},l)$ rod at $\Delta E=2$ meV. At this energy one sees not only the structure factor modulation, as in Fig. 9, but also the effects of dispersion. At 2 meV one crosses through the middle of the

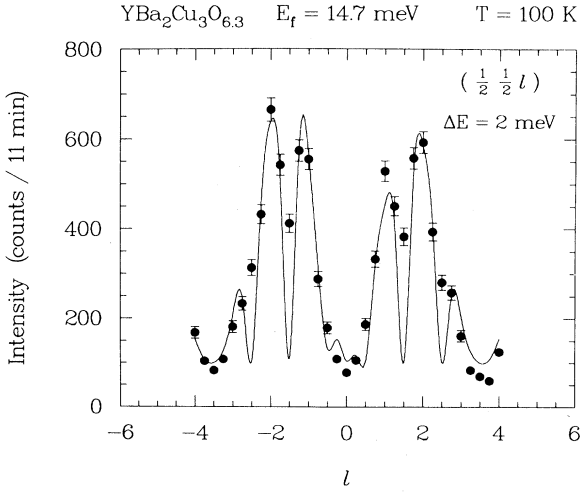

FIG. 12. Scan along the 2D rod at an energy transfer of 2 meV. The solid line was calculated as discussed in the text. The modulation is due to a combination of the inelastic structure factor and dispersion effects.

in-plane acoustic mode spin-wave branch. The calculated curve takes the dispersion into account, and it is in quite reasonable agreement with the measured points.

V. TEMPERATURE-DEPENDENT EFFECTS

The temperature dependence of the $(\frac{1}{2},\frac{1}{2},-2)$ magnetic Bragg peak is reproduced in Fig. 13(a). There are two separate regions of interest: (1) near the Néel temperature, and (2) at low temperatures where the peak intensity begins to decrease. We will first consider behavior near the ordering temperature, and then turn to the low-temperature regime.

In La_2CuO_4 it is well established[8,9] that the Cu spins within individual CuO_2 layers remain correlated over many lattice spacings at temperatures well above the 3D ordering transition due to the extremely large intraplanar superexchange. The scans along $(\frac{1}{2},\frac{1}{2},l)$ at 290 and 350 K displayed in Fig. 9 clearly show that in $YBa_2Cu_3O_{6.3}$ the spins not only in a single layer but in bilayers remain correlated well above T_N. Thus, the correlation length with in a bilayer must be quite large above T_N, and 3D ordering occurs when interbilayer correlations develop.

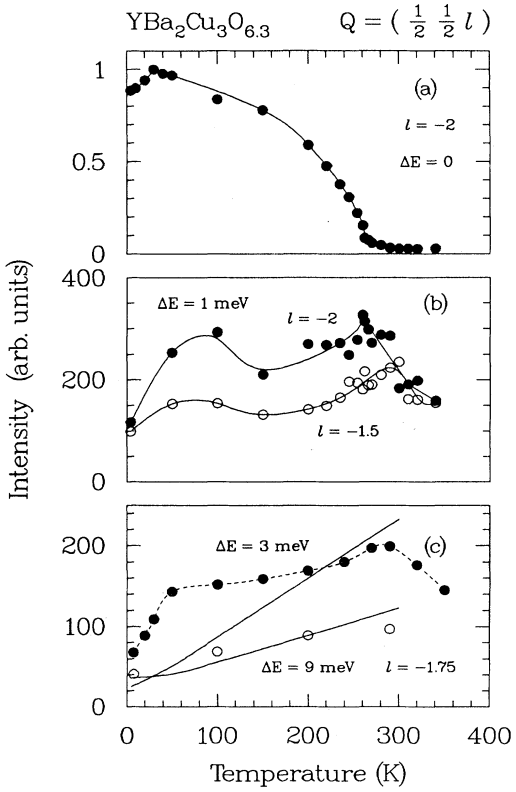

FIG. 13. Temperature dependence of elastic and inelastic magnetic scattering in $YBa_2Cu_3O_{6+x}$. (a) Elastic Bragg peak intensity at $(\frac{1}{2},\frac{1}{2},-2)$. (b) Inelastic intensity for $\Delta E=1$ meV at $(\frac{1}{2},\frac{1}{2},-2)$ and $(\frac{1}{2},\frac{1}{2},-1.5)$. (c) Background-corrected inelastic intensity at $(\frac{1}{2},\frac{1}{2},-1.75)$ for $\Delta E=3$ and 9 meV. The solid lines represent the calculated temperature dependence normalized to the 9-meV point at 200 K, taking the spectrometer resolution function into account; the dashed line is a guide to the eye.

In Fig. 11(b) the constant-**Q** scan at 320 K indicates that the anisotropy resulting in the gap for out-of-plane fluctuations may still be important above T_N. We expect that the anisotropy will be important as long as the correlation length within a CuO_2 layer is significant. Such behavior may not be unusual, as it appears that the existence of an anisotropy gap has been observed well above T_N in the compound CuO. The gap in the antiferromagnetically ordered phase of CuO has been measured by neutron scattering[35] to be approximately 2.5 meV. Because of the large gap, no magnetic absorption was observed in antiferromagnetic resonance measurements[36] at microwave frequencies at temperatures less than $2T_N$.

In order to study the development of 3D dispersion, we measured the scattered intensity for $\Delta E=1$ meV at the spin-wave zone center and zone-boundary points $(\frac{1}{2},\frac{1}{2},-2)$ and $(\frac{1}{2},\frac{1}{2},-1.5)$, respectively. The results are shown in Fig. 13(b). With decreasing temperature, the zone-boundary intensity peaks near 290 K and then starts to decrease. Note that weak elastic scattering first appears at $\sim$290 K in Fig. 13(a). At the zone-center point the 1 meV scattering peaks more or less at $T_N=260$ K. Hence, it seems that 3D dispersion first appears near 290 K, but long-range order does not set in until a temperature 30 K lower. We do not know to what extent this behavior is dependent on the oxygen content of the compound.

Next we discuss the low-temperature regime. In Fig. 13(a) one can see that the magnetic Bragg peak intensity has a maximum at 30 K, and that it decreases below that temperature. A similar behavior was reported by Kadowaki *et al.*[14] in an $YBa_2Cu_3O_{6+x}$ crystal with $x\sim0.35$; however, with their crystal they saw new superlattice peaks appear at $(\frac{1}{2},\frac{1}{2},L+\frac{1}{2})$ when the $(\frac{1}{2},\frac{1}{2},L)$ intensity began to decrease. The extra reflections occurred due to ordering of moments at Cu(1) sites. Figure 14(a) shows a scan at 4.5 K of elastic scattering along $(\frac{1}{2},\frac{1}{2},l)$ between the $(\frac{1}{2},\frac{1}{2},-2)$ and $(\frac{1}{2},\frac{1}{2},-1)$ magnetic peaks; a scan measured at 50 K has been subtracted off in order to eliminate contamination from $BaCuO_2$ impurities. Instead of a Bragg-type superlattice peak at $(\frac{1}{2},\frac{1}{2},-\frac{3}{2})$, we observe diffuse scattering distributed all along the 2D rod, but peaking at the l=integer peak positions. Thus, at 4.5 K we observe a superposition of Bragg peaks at $(\frac{1}{2},\frac{1}{2},L)$ and the diffuse 2D scattering. At least qualitatively it appears that below 30 K elastic scattering intensity is transferred from the Bragg peaks to the 2D rod. As can be seen in Fig. 14(b), the intensity of the diffuse scattering is also modulated by the structure factor determined by antiferromagnetic coupling of the CuO_2 bilayers. Similar observations were reported by Rossat-Mignod *et al.*[4] in a crystal of identical oxygen content ($x=0.3$).

Associated with the change in elastic scattering, we also see some anomalous inelastic effects. For example, the intensity at zone center and $\Delta E=1$ meV shown in Fig. 13(b) shows an enhancement around 50–100 K. Figure 13(c) shows background-corrected intensities measured at $\mathbf{Q}=(\frac{1}{2},\frac{1}{2},-1.75)$ for $\Delta E=3$ and 9 meV. The solid lines indicate the temperature dependence calculat-

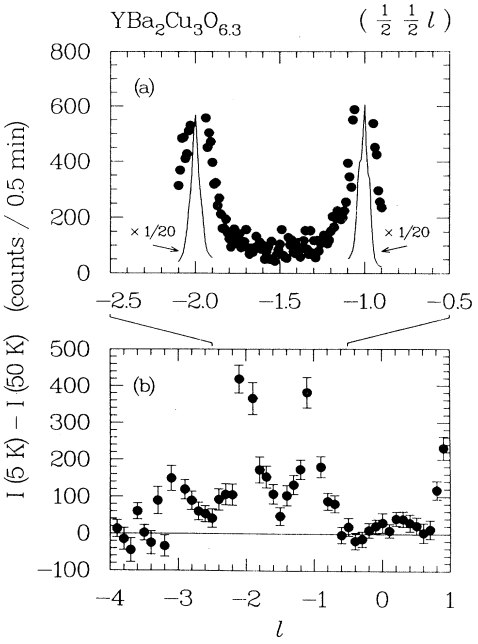

FIG. 14. Difference in elastic intensity along the 2D rod $(\frac{1}{2},\frac{1}{2},l)$ between 4.5 and 50 K. (a) Scattering between the Bragg peaks at $l=-2$ and -1; solid lines represent Bragg scattering at 4.5 K, scaled by $\frac{1}{20}$. (b) Measurement over a wider range of l.

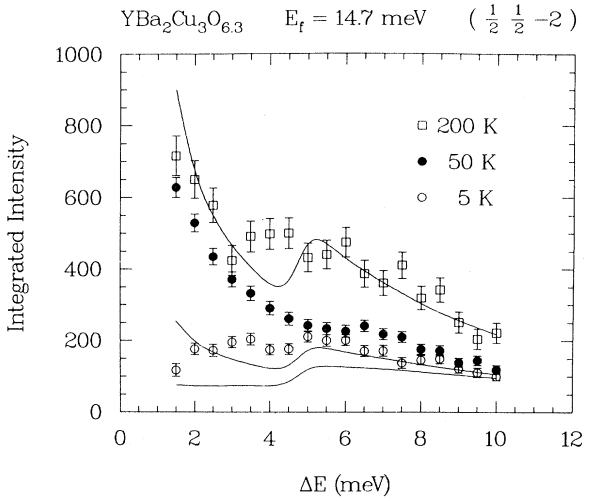

FIG. 15. Constant-Q scans at magnetic zone center point $(\frac{1}{2},\frac{1}{2},-2)$ at temperatures of 4.5, 50, and 200 K. The solid lines are calculated intensities using the parameters determined from measurements at 200 K and normalized to the 200-K data, as discussed in the text.

ed using the exchange couplings determined at 200 K and fixing the amplitude factor to fit the 9-meV point at 200 K. The scattering at 9 meV is in reasonable agreement with the expected temperature dependence; however, the 3-meV data shows a large enhancement which seems to peak near 50 K.

The energy dependence of the anomaly is further demonstrated in Fig. 15, which presents measurements of inelastic scattering at $\mathbf{Q}=(\frac{1}{2},\frac{1}{2},-2)$ for temperatures of 4.5, 50, and 200 K. The solid curves are calculated from the spin-wave model with the amplitude adjusted to fit the 200-K data. One can clearly see that at 50 K there is a large amount of excess scattering at low energies. The discrepancy with the calculation is smaller but still significant at 4.5 K.

Although we do not see them order in a coherent fashion, we expect that a finite fraction of the Cu(1) atoms should be magnetic. Johnston *et al.*[15] first noted a paramagnetic, Curie-type contribution from these moments in susceptibility measurements. In a recent study, Farneth *et al.*[16] found that the paramagnetic contribution from $Cu(1)^{2+}$ decreases sharply below 20–30 K. Freezing of the moments due to coupling with CuO_2 planes would explain the disappearance of paramagnetic susceptibility. An incoherent ordering of Cu(1) and Cu(2) layers can also explain the lack of superlattice peaks and the appearance of diffuse scattering in the neutron measurements.

Schematic diagrams of magnetic structures are depicted in Fig. 16. In (a) the usual type-I antiferromagnetic ordering of the CuO_2 bilayers is indicated by full and empty bars. In (c) the type-II ordering involving Cu(1) layers, indicated by broken bars, observed by Kadowaki *et al.*[14] is shown. A mixture of the two structures is shown in (b), in which the order is dominantly of type-I with isolated single layers of type-II structure which act like antiphase boundaries. Such a random mixture of the two types of magnetic structure would explain the decrease in the type-I order parameter at low temperature, the lack of type-II superlattice peaks, and the appearance of 2D scattering peaked around the type-I Bragg peak positions. The excess low-energy inelastic scattering which peaks near the low-temperature magnetic transi-

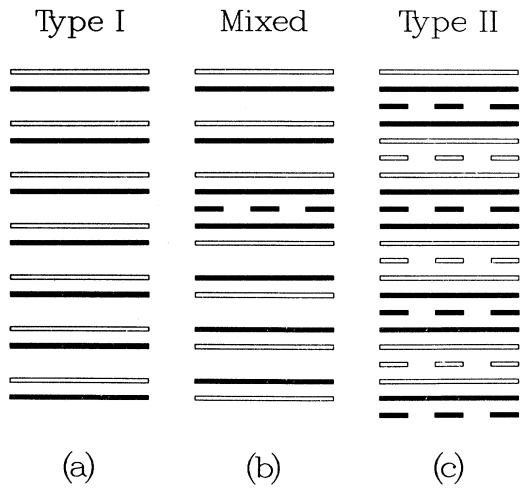

FIG. 16. Schematic diagrams of different magnetic structures, as discussed in the text. Each bar represents an antiferromagnetic CuO_2 plane in which the Cu spins have a simple Néel order. Black and white bars indicate layers with antiparallel spins. Dashed bars represent magnetically ordered Cu(1) layers.

tion is presumably due to critical slowing of the $Cu(1)^{2+}$ moments. Such an interpretation is consistent with the observation[37] of a divergence in $1/T_2$ at 20 K for $Cu(1)^{1+}$ sites in nuclear quadrupole resonance (NQR) measurements in a sample with $x=0.3$.

The mixed ordering shown in Fig. 16(b) is not the only type of magnetic structure defect expected in a crystal with $x\sim0.3$. Monte Carlo simulations by Lu and Patton[38] indicate that in order to explain the observed decrease in T_N for $x\gtrsim0.2$, magnetic defects in the CuO_2 layers are required, as well as the frustrating effects of Cu(1) moments. An O $2p$ hole is expected to align the moments on the neighboring two copper sites ferromagnetically,[7,22,39] causing a disruption of the antiferromagnetic order. We know that in La_2CuO_4 a very low density of mobile holes kills the long-range magnetic order. The gradual variation of T_N between $x\sim0.2$ and 0.4 indicates that holes present in the CuO_2 planes of $YBa_2Cu_3O_{6+x}$ must be fairly well localized.

That a small number of holes should be present seems quite reasonable. In the orthorhombic phase the O atoms in the Cu(1) layer tend to order in chains, and one hole is induced for each oxygen in a chain.[21] It has been suggested[40] that the O atoms should also cluster into chain segments in the tetragonal phase, the random orientations of the segments resulting in the macroscopic tetragonal symmetry. As is well known, the oxygen content at which the orthorhombic-tetragonal transition occurs depends on sample preparation conditions. Nakazawa and Ishikawa[41] have recently shown that $YBa_2Cu_3O_{6+x}$ can retain its orthorhombic structure down to $x\sim0.2$. Hence, it seems quite likely that Cu-O chain segments are present in the tetragonal phase at least for $x\gtrsim0.2$. The number of holes per chain oxygen will be reduced because of end effects, but some should be present in any case.

An isolated $Cu(1)^{2+}$ coupled to its Cu(2) neighbors would have to flip the spin of one of the Cu(2) spins, resulting in a defect similar to that of a localized O $2p$ hole in a CuO_2 plane. Actually, we expect the $Cu(1)^{2+}$ ions should come in pairs surrounding a bridging oxygen. The disruption of the antiferromagnetic order can be minimized, along with the energy, by combining Cu(1) moments and O $2p$ holes in a configuration such as that shown in Fig. 17. The minimal energy of such a configuration would tend to localize the holes, and hence prevent the destruction of long-range order. The flipping of some Cu(2) spins would, however, lead to a reduction in the order parameter, as observed experimentally.[3,4]

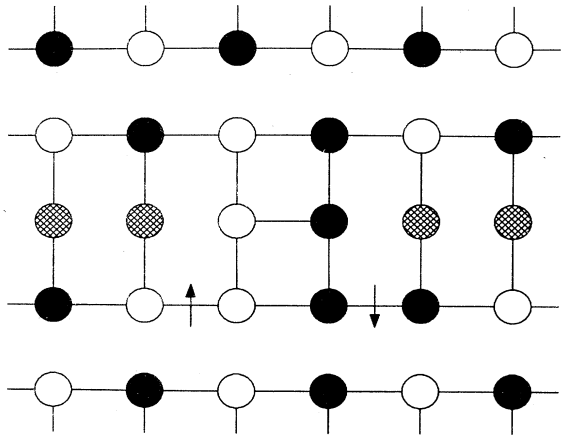

FIG. 17. Possible magnetic defect structure for $0.2<x<0.4$. Solid and open circles indicate Cu moments with antiparallel spins; the cross-hatched circles indicate $Cu(1)^{1+}$. Line segments represent bridging oxygens. The two arrows represent O $2p$ holes; the orientation of the arrows is arbitrary.

VI. SUPERCONDUCTING CRYSTALS

Neutron diffraction measurements on the superconducting crystals with $x\gtrsim0.45$ listed in Table II indicate that they have no magnetic order down to 5–10 K. More specifically, we have found no sign of any Bragg peaks at $(\frac{1}{2},\frac{1}{2},L)$ or $(\frac{1}{2},\frac{1}{2},L+\frac{1}{2})$ positions. Assuming that the ordering would be the same as for small x samples, we should be able to detect peaks corresponding to an average moment of $\sim0.01\mu_B/Cu^{2+}$. This result is in sharp contrast to a report by Petitgrand and Colin[42] of the coexistence of antiferromagnetism and superconductivity in a sample with $x=0.55$. Our negative result suggests that such a coexistence is not an intrinsic behavior.

We have also looked for inelastic scattering from magnetic excitations in these crystals. Most of the measurements have been made at energy transfers of 3 and 6 meV over a range of temperatures 5–300 K. No scattering with the expected 2D symmetry could be identified. Although the sizes of the crystals vary, it should be relatively easy to see inelastic magnetic scattering if the cross section were comparable to that observed in the magnetically ordered $x=0.3$ crystal. All we can conclude at this point is that the low-energy magnetic cross section along the 2D scattering rod is much smaller than that observed in the tetragonal phase. Our observations are consistent with the negligible magnetic scattering integrated over $|\hbar\omega|<25$ meV found in $YBa_2Cu_3O_7$ by Brückel *et al.*[43]

What are the implications of these negative results? One possibility is that there are no magnetic moments present in the superconducting, orthorhombic phase of $YBa_2Cu_3O_{6+x}$; however, there are many other experimental results which argue against such a conclusion. First of all, muon spin relaxation[2] (μSR) and nuclear quadrupole resonance[44] studies indicate that, although the staggered magnetization measured by neutron diffraction decreases with increasing x, the local moment remains constant, at least in the tetragonal phase. Secondly, magnetic susceptibility measurements[15,16] indicate a very gradual change in magnetic properties on crossing the tetragonal-orthorhombic phase boundary. Furthermore, light scattering studies indicate that magnetic correlations are still present in the orthorhombic phase.[13]

If magnetic correlations do exist in the superconducting phase, the correlation length is certainly quite short. The decrease in correlation length on going from the tetragonal to the orthorhombic phase should cause sharp spin-wave excitations to broaden considerably; hence,

even if the integrated intensity is constant, the cross section at a given point in reciprocal space should be expected to decrease by a significant amount. In $La_{2-x}Sr_xCuO_{4-y}$, the maximum cross section for a given excitation energy is found to decrease by almost an order of magnitude due to such correlation length effects.[45] It is also possible that the spectral distribution may be modified when holes are present, thus depressing the low-energy cross section.

We believe that magnetic fluctuations should be present and detectable in superconducting $YBa_2Cu_3O_{6+x}$. The problem is to locate the associated inelastic scattering in $(\mathbf{Q},\omega,T)$ space. Mezei *et al.*[46] have observed some low energy diffuse magnetic scattering in a powder sample with $x=0.59$ using a neutron spin-echo spectrometer. Very recently we have seen reasonably strong spin-wave-like scattering in a large orthorhombic crystal with $x\sim0.45$ and $T_c\approx15$ K. (Detailed results will be reported elsewhere.) Much more work is required to properly characterize magnetic fluctuations in orthorhombic $YBa_2Cu_3O_{6+x}$ and any relationship they may have to superconductivity.

VII. SUMMARY

We have used neutron scattering to study magnetic excitations in single crystals of $YBa_2Cu_3O_{6+x}$. Most of the results reported here are for a large antiferromagnetic crystal with $x\sim0.3$. A simple linear spin-wave model has been developed and used to interpret the inelastic scattering measurements. The Cu(1) sites were initially ignored, and the magnetic lattice was assumed to consist of just the $Cu(2)^{2+}$ atoms. Because of the non-Bravais nature of this sublattice, the spin waves are split into acoustic and optical modes. A weak anisotropy due to spin-orbit coupling within the CuO_2 layers causes an energy gap for spin fluctuations out of the plane, thus resulting in a splitting of the doubly degenerate acoustic and optical modes into in-plane and out-of-plane branches. We carefully studied the acoustic modes. As in La_2CuO_4,[8,9] a very large intraplanar superexchange is found: $J_{\parallel}=80^{+60}_{-30}$ meV. This result is quite consistent with the value of 120 meV obtained from Raman scattering measurements of two-magnon excitations.[13] The direct exchange between Cu atoms in nearest-neighbor CuO_2 planes is also surprisingly strong. As a result, the optical-mode energies are above 30 meV, and we estimate $J_{\perp1}\gtrsim2$ meV. Dispersion of the in-plane acoustic mode is observable, and from it a value of $J_{\perp2}=0.020\pm0.005$ meV is obtained, corresponding to the coupling between next-nearest-neighbor planes. For the anisotropy, we find $D=0.035\pm0.005$ meV.

Above T_N, the CuO_2 bilayers are still strongly coupled. Three-dimensional ordering occurs when interbilayer correlations develop; however, it appears that 3D dispersion may develop at a temperature 30 K higher than the onset of long-range order. Magnetic moments of Cu(1) sites appear to become important at low temperature. Below 30 K the magnetic order parameter begins to decrease, and diffuse scattering appears along the 2D scattering rod. This behavior is explained by assuming that the Cu(1) moments order in an incoherent fashion, resulting in a mixture of the usual type-I ordering with some layers of the type-II structure first observed by Kadowaki *et al.*[14] Excess low-energy inelastic scattering is found to peak in intensity near the structural transition, and it is apparently due to critical slowing in the Cu(1) moments.

We have searched for low-energy inelastic scattering from magnetic fluctuations in several superconducting single crystals of $YBa_2Cu_3O_{6+x}$, but so far we have not been able to identify any. If the cross section were identical to that in the antiferromagnetic regime, we should have seen something; however, with the lack of long-range order, it seems quite likely that magnetic fluctuations should have a broader distribution in reciprocal space, thus making them more difficult to see. Further studies are continuing on new and larger superconducting crystals.

ACKNOWLEDGMENTS

We gratefully acknowledge helpful discussions with J. D. Axe, R. J. Birgeneau, V. J. Emery, M. Kastner, Y. Lu, B. R. Patton, and S. K. Sinha. This work was supported in part by the U.S.-Japan Cooperative Neutron Scattering Program and a Grant-In-Aid for Special Project Research from the Japanese Ministry of Education, Science and Culture. Research at Brookhaven is supported by the Division of Materials Sciences, U.S. Department of Energy under Contract No. DE-AC02-76CH00016. Work at the Massachusetts Institute of Technology is supported by the National Science Foundation under Contract No. DMR85-01856 and DMR84-18718.

[1] D. Vaknin, S. K. Sinha, D. E. Moncton, D. C. Johnston, J. Newsam, C. R. Safinya, and H. E. King, Jr., Phys. Rev. Lett. **58**, 2802 (1987); D. C. Johnston, J. P. Stokes, D. P. Goshorn, and J. T. Lewandowski, Phys. Rev. B **36**, 4007 (1987); J. I. Budnick, B. Chamberland, D. P. Yang, Ch. Niedermayer, A. Golnik, E. Recknagel, M. Rossmanith, and A. Weidinger, Europhys. Lett. **5**, 651 (1988); Y. Kitaoka, K. Ishida, S. Hiramatsu, and K. Asayama, J. Phys. Soc. Jpn. **57**, 734 (1988).

[2] J. H. Brewer *et al.*, Phys. Rev. Lett. **60**, 1073 (1988).

[3] J. M. Tranquada, D. E. Cox, W. Kunnmann, H. Moudden, G. Shirane, M. Suenaga, P. Zolliker, D. Vaknin, S. K. Sinha, M. S. Alvarez, A. J. Jacobson, and D. C. Johnston, Phys. Rev. Lett. **60**, 156 (1988); J. M. Tranquada, A. H. Moudden, A. I. Goldman, P. Zolliker, D. E. Cox, G. Shirane, S. K. Sinha, D. Vaknin, D. C. Johnston, M. S. Alvarez, A. J. Jacobson, J. T. Lewandowski, and J. M. Newsam, Phys. Rev. B **38**, 2477 (1988).

[4] J. Rossat-Mignod, P. Burlet, M. J. Jurgens, C. Vettier, L. P. Regnault, J. Y. Henry, C. Ayache, L. Forro, H. Noel, M. Po-

tel, P. Gougeon, and J. C. Levet, J. Phys. (Paris) Colloq. **49**, C8-2119 (1988); M. J. Jurgens, P. Burlet, C. Vettier, L. P. Regnault, J. Y. Henry, J. Rossat-Mignod, H. Noel, M. Potel, P. Gougeon, and J. C. Levet, Physica B **156&157**, 846 (1989).

[5]B. X. Yang *et al.*, Phys. Rev. B **39**, 847 (1989); N. Nishida, H. Miyatake, S. Okuma, T. Tamegai, Y. Iye, R. Yoshizaki, K. Nishiyama, and K. Nagamine, Physica C **156**, 625 (1988).

[6]J. Mizuki, Y. Kubo, T. Manako, Y. Shimakawa, H. Igarashi, J. M. Tranquada, Y. Fujii, L. Rebelsky, and G. Shirane, Physica C **156**, 781 (1988).

[7]A. Aharony, R. J. Birgeneau, A. Coniglio, M. A. Kastner, and H. E. Stanley, Phys. Rev. Lett. **60**, 1330 (1988).

[8]G. Shirane, Y. Endoh, R. J. Birgeneau, M. A. Kastner, Y. Hidaka, M. Oda, M. Suzuki, and T. Murakami, Phys. Rev. Lett. **59**, 1613 (1987).

[9]Y. Endoh *et al.*, Phys. Rev. B **37**, 7443 (1988); R. J. Birgeneau *et al.*, *ibid.* **38**, 6614 (1988).

[10]Y. J. Uemura *et al.*, Physica C **153-155**, 769 (1988); D. R. Harshman, G. Aeppli, G. P. Espinosa, A. S. Cooper, J. P. Remeika, E. J. Ansaldo, T. M. Riseman, D. Ll. Williams, D. R. Noakes, B. Ellman, and T. F. Rosenbaum, Phys. Rev. B **38**, 852 (1988); A. Weidinger, Ch. Niedermayer, A. Golnik, R. Simon, E. Recknagel, J. I. Budnick, B. Chamberland, and C. Baines, Phys. Rev. Lett. **62**, 102 (1988).

[11]All reciprocal lattice vectors in this paper are specified in terms of reciprocal lattice units.

[12]M. Sato, S. Shamoto, J. M. Tranquada, G. Shirane, and B. Keimer, Phys. Rev. Lett. **61**, 1317 (1988).

[13]K. B. Lyons, P. A. Fleury, L. F. Schneemeyer, and J. V. Waszczak, Phys. Rev. Lett. **60**, 732 (1988).

[14]H. Kadowaki, M. Nishi, Y. Yamada, H. Takeya, H. Takei, S. M. Shapiro, and G. Shirane, Phys. Rev. B **37**, 7932 (1988).

[15]D. C. Johnston, S. K. Sinha, A. J. Jacobson, and J. M. Newsam, Physica **153-155**, 572 (1988).

[16]W. E. Farneth, R. S. McLean, E. M. McCarron, III, F. Zuo, Y. Lu, B. R. Patton, and A. J. Epstein, Phys. Rev. B **39**, 6594 (1989).

[17]T. Takabatake, M. Ishikawa, and T. Sugano, Jpn. J. Appl. Phys. **26**, L1859 (1987); K. Westerholt and H. Bach, Phys. Rev. B **39**, 858 (1989).

[18]K. B. Lyons, P. A. Fleury, L. F. Schneemeyer, and J. V. Waszczak, Phys. Rev. Lett. **60**, 732 (1988).

[19]C. Herring, in *Magnetism*, edited by G. T. Rado and H. Suhl (Academic, New York, 1966), Vol. II B, p. 1.

[20]A. J. Freeman and R. E. Watson, Phys. Rev. **124**, 1439 (1961).

[21]J. M. Tranquada, S. M. Heald, A. R. Moodenbaugh, and Y. Xu, Phys. Rev. B **38**, 8893 (1988).

[22]Y. Guo, J.-M. Langlois, W. A. Goddard III, Science **239**, 896 (1988).

[23]A. H. Moudden, G. Shirane, J. M. Tranquada, R. J. Birgenau, Y. Endoh, K. Yamada, Y. Hidaka, and T. Murakami, Phys. Rev. B **38**, 8720 (1988).

[24]J. H. Van Vleck, J. Phys. Radium **12**, 262 (1951).

[25]T. Nagamiya, K. Yosida, and R. Kubo, Adv. Phys. **4**, 1 (1955).

[26]J. Owen and E. A. Harris, in *Electron Paramagnetic Resonance*, edited by S. Geschwind (Plenum, New York, 1972), Chap. 6.

[27]G. J. Bowden, P. R. Elliston, K. T. Wan, S. X. Dou, K. E. Easterling, A. Bourdillon, C. C. Sorrell, B. A. Cornell, and F. Separovic, J. Phys. C **20**, L545 (1987).

[28]C. Kittel, *Quantum Theory of Solids* (Wiley, New York, 1963), Chap. 4.

[29]W. Marshall and R. D. Lowde, Rep. Prog. Phys. **31**, 705 (1968); S. W. Lovesey, *Theory of Neutron Scattering from Condensed Matter* (Clarendon, Oxford, 1984), Vol. 2.

[30]R. M. Moon, T. Riste, and W. C. Koehler, Phys. Rev. **181**, 920 (1969); K. R. A. Ziebeck and P. J. Brown, J. Phys. F **10**, 2015 (1980).

[31]R. J. Papoular and G. Collin, Phys. Rev. B **38**, 768 (1988).

[32]S. Shamoto, S. Hosoya, and M. Sato, Solid State Commun. **66**, 195 (1988).

[33]D. C. Johnston, A. J. Jacobson, J. M. Newsam, J. T. Lewandowski, D. P. Goshorn, D. Xie, and W. B. Yelon, in *Chemistry of High-Temperature Superconductors*, edited by D. L. Nelson, M. S. Whittingham, and T. F. George, ACS Symposium Series No. 351 (American Chemical Society, Washington, D.C., 1987); W. R. McKinnon, M. L. Post, L. S. Selwyn, G. Pleisier, J. M. Tarascon, P. Barboux, L. H. Greene, and G. W. Hull, Phys. Rev. B **38**, 6543 (1988); R. J. Cava, B. Batlogg, C. H. Chen, E. A. Rietman, S. M. Zahurak, and D. Werder, *ibid.* **36**, 5719 (1987); A. Manthiram, J. S. Swinnea, Z. T. Sui, H. Steinfink, and J. B. Goodenough, J. Am. Chem. Soc. **109**, 6667 (1987).

[34]R. A. Cowley, G. Shirane, R. J. Birgeneau, and H. J. Guggenheim, Phys. Rev. B **15**, 4292 (1977).

[35]B. X. Yang, T. R. Thurston, J. M. Tranquada, and G. Shirane, Phys. Rev. B **39**, 4343 (1989).

[36]L. R. Maxwell and T. R. McGuire, Rev. Mod. Phys. **25**, 279 (1953); F. Mehran, S. E. Barnes, G. V. Chandrasekhar, T. R. McGuire, and M. W. Shafer, Solid State Commun. **67**, 1187 (1988).

[37]Y. Kitaoka, S. Hiramatsu, K. Ishida, K. Asayama, H. Takagi, H. Iwabuchi, S. Uchida, and S. Tanaka, J. Phys. Soc. Jpn. **57**, 737 (1988).

[38]Y. Lu and B. R. Patton (unpublished).

[39]V. J. Emery and G. Reiter, Phys. Rev. B **38**, 4547 (1988).

[40]A. Renault, J. K. Burdett, and J.-P. Pouget, J. Solid State Chem. **71**, 587 (1987).

[41]Y. Nakazawa and M. Ishikawa, Physica C **158**, 381 (1989).

[42]D. Petitgrand and G. Collin, Physica B **156&157**, 858 (1989).

[43]T. Brückel, H. Capellmann, W. Just, O. Schärpf, S. Kemmler-Sack, R. Kiemel, and W. Schaefer, Europhys. Lett. **4**, 1189 (1987).

[44]M. Matsumura, H. Yamagata, Y. Yamada, K. Ishida, Y. Kitaoka, K. Asayama, H. Takagi, H. Iwabuchi, and S. Uchida, J. Phys. Soc. Jpn. **57**, 3297 (1988); P. Mendels and H. Alloul, Physica C **156**, 355 (1988).

[45]G. Shirane, R. J. Birgeneau, Y. Endoh, P. Gehring, M. A. Kastner, K. Kitazawa, H. Kojima, I. Tanaka, T. R. Thurston, and K. Yamada, Phys. Rev. Lett. **63**, 330 (1989).

[46]F. Mezei, B. Faragó, C. Pappas, Gy. Hutiray, L. Rosta, and L. Mihály, Physica C **153-155**, 1669 (1988).